SIViP
DOI 10.1007/s11760-009-0117-4

ORIGINAL PAPER

No-reference assessment of blur and noise impacts on image quality

Erez Cohen · Yitzhak Yitzhaky

Received: 17 December 2007 / Revised: 9 February 2009 / Accepted: 18 April 2009

Abstract The quality of images may be severely degraded in various situations such as imaging during motion, sensing through a diffusive medium, and low signal to noise. Often in such cases, the ideal un-degraded image is not available (no reference exists). This paper overviews past methods that dealt with no-reference (NR) image quality assessment, and then proposes a new NR method for the identification of image distortions and quantification of their impacts on image quality. The proposed method considers both noise and blur distortion types that may exist in the image. The same methodology employed in the spatial frequency domain is used to evaluate both distortion impacts on image quality, while noise power is further independently estimated in the spatial domain. Specific distortions addressed here include additive white noise, Gaussian blur and de-focus blur. Estimation results are compared to the true distortion quantities, over a set of 75 different images.

Keywords Image quality measure · No-reference IQM · Image quality assessment · Image power spectrum · Blur impact · Noise impact

1 Introduction

Image signals can be degraded by a variety of causes during acquisition, transmission, storage and reconstruction. Identifying the distortion factor and quantifying its impact on the image may be useful for various applications such as improving the acquisition system and thus the quality of the produced image.

E. Cohen · Y. Yitzhaky (✉)
Department of Electro-Optics Engineering,
Ben-Gurion University, POB 653, 84105 Beer-Sheva, Israel
e-mail: itzik@ee.bgu.ac.il

The quality of an image is mainly defined by the image's customer due to its preference [1]. Therefore, in many applications, human viewers involved in subjective measurements, are considered to provide the ultimate judgment of image quality [2]. While subjective assessment, based on perceived results, is considered a reliable image quality measure (IQM), it has disadvantages such as cost, slowness, it depends on viewing conditions and vision capabilities, and its results are difficult to be reproduced. It is also not necessarily most reliable for computer vision applications which do not have the characteristics of the human visual system (HVS). Objective quality metrics account for these drawbacks since they produce immediate results without human involvement. The goal of *visual* objective quality metrics is to quantify the image quality automatically and to obtain reliable results that are well correlated with subjective assessments. However, the end purpose of an IQM may be non-visual in the sense that the end user of the image may be not a human, but a computer vision process, for instance.

Objective IQM methods can be classified by whether a reference image, representing the original signal exists. When such a reference is accessible, the quality can be evaluated by comparison measurement of the differences between the evaluated image and the reference one. This kind of measurements is known as a full-reference (FR) image quality assessment of image *similarity* or *fidelity* [3]. Over the years, numerous reference-based IQM methods have been proposed, largely summarized in several review articles [2,4–6]. Another IQM approach is the reduced-reference (RR) quality assessment, which assumes that partial information about the reference signal is available and used for the quality evaluation. In many applications, where a reference image cannot be provided, FR and RR IQMs cannot be used, and a no-reference (NR) quality assessment is required, intending to blindly (without any reference) quantify the

Published online: 19 May 2009

distortion severity in the image. Although the original image is frequently not available, the vast majority of objective IQM techniques are FR.

The common noise and blur image distortions may be caused in different ways. Blur may result during image acquisition by causes such as the limited bandwidth of the imager, motion during exposure, out-of-focus or atmospheric turbulence [7,8]. The difficulty in assessing both noise and blur when exist together in the image is derived from their contradicting effects on image properties. In the frequency domain, noise affects the whole frequency band and mainly increases the higher-frequencies, while blur mainly suppresses the higher-frequencies. Due to this feature, many objective image quality assessment methods are specified only to one of these impairments ignoring the other.

The purpose of this work is to efficiently evaluate the *distortion impact* on image quality with the ability of quantifying such different types of image impairments which may exist in the image. A distortion (such as blur) impact may be an IQM if it solely degrades the image. This paper proposes an NR objective method to assess distortion impact on a natural image and thus on its relative quality, considering noise and blur. A natural image, which represents ordinary human visual stimulus, has some consistent statistical properties [9]. The method assumes common statistics of natural images, which can be observed at their power spectra. Manipulations performed with the distorted image spectrum enhance the appearance of the distortion effects, and thus facilitate a reliable distortion impact assessment that corresponds to the true distortion used to degrade the image.

The rest of this paper is organized as follows: Sect. 2 describes spectral properties of natural images. Section 3 gives an overview of NR IQM methods. Section 4 introduces the proposed method, and results are presented in Sect. 5. Conclusions are in Sect. 6.

2 Spectral properties of natural images

Natural scenes represent natural visual stimulus of the eye [10]. Therefore, almost all images, taken in daily applications, can be considered as natural. Figure 1 presents 16 examples of natural images taken from a set of 75 test images used in this work. The whole image set is available on the web [11]. Some empirical evidences support the idea that human spatial vision is optimized to natural images and therefore expects to interpret images that conform to natural image statistics [12–14].

The structure of a natural image reveals consistent statistical properties that reflect some of its typical properties [9]. Natural image statistics can be classified by their order [10,12,13]. First order statistics consider each location in the image independently, second order statistics include two separate positions dependency, and higher order statistics describe mutual relations between three or more positions in the image. The most popular second order statistics representations of a natural image are the *autocorrelation* function defining the correlation between two points in an image, and the *power spectrum* derived from the Fourier transform of the autocorrelation function [15]. An $M \times M$ pixels image normalized power spectrum $P(u, v)$ can be obtained by [10, 13,16,17]:

$$P(u, v) = \frac{|F(u, v)|^2}{M^2}, \tag{1}$$

where F is the Fourier transform of the image, (u, v) are the two-dimensional spatial frequency coordinates and M^2 is the total number of pixels in the image. It has been found out that when presenting the power spectrum of a natural image (averaged with respect to the angle) as a function of frequency, it behaves approximately with the form [7,10,13,14,18–20]:

$$P(f) \propto \frac{1}{f^{\gamma}}, \tag{2}$$

where f is spatial frequency and γ is a spectral slope. The average power spectral slope of natural images obtained in different studies varies subtly ($1.8 \leq \gamma \leq 2.3$ in [9], $1.45 \leq \gamma \leq 2.31$ in [10], $1.46 \leq \gamma \leq 2.3$ in [13], $1.4 \leq \gamma \leq 3.2$ in [14]s, $1.83 \leq \gamma \leq 2.22$ in [18], $1.4 \leq \gamma \leq 3$ in [20]). Most of the studies yielded an average slope around 2. A non-isotropic image mean power spectrum (using polar coordinates) can be presented in a more general form as a function of orientation (angle):

$$P(f, \theta) \propto \frac{1}{f^{\gamma(\theta)}}, \tag{3}$$

where $\gamma(\theta)$ is the spectral slope as a function of orientation (averaged with respect to θ angle). Some studies have shown that the averaged oriented power spectrum has frequently a vertical or horizontal preferred orientation [10,13,18,19].

Other image models such as the exponential (separable or non-separable) covariance [21], produce eventually a similar monotonically decreasing spectral behavior, in which higher spatial frequency components contain lower energy. This common statistical behavior is employed in this work for the identification of blur and noise distortions in the image.

3 Overview of NR image quality measurement methods

As stated earlier, in many applications a reference image is unavailable and therefore a comparative image quality measurement is impossible. In these cases, the image quality should be blindly evaluated. Generally, NR quality assessment methods (also named *blind* assessments) attempt to

Fig. 1 Examples of natural images from the test set. The whole image set is available on the web [11]

quantify the distortion that may exist in the evaluated image assuming common properties of the original (natural) image. Most of the objective NR quality assessment methods are numerical measures, where image quality score is determined by a ranking scale, while others employ graphical measures specified to quantify the distortions in the evaluated image [3,4,6]. NR image quality evaluations were carried out either in the frequency domain [17,22,23] or in the spatial domain (image plane) [24–35]. A brief overview of some NR quantitative IQM techniques, differ in their approaches and implementations, is presented subsequently.

3.1 NR quality measures in the frequency domain

The common statistical characteristics of the power spectra of natural images may be useful in the image quality evaluation process. Spectral measures, obtained in the frequency domain, consider the distortion impact on the evaluated image power spectrum.

Saghri et al. [22] proposed an IQM based on HVS model for compressed images. The measure is performed in the spatial frequency domain, incorporating the HVS model in the DCT (discrete cosine transform) domain. The algorithm considers HVS sensitivities to background illumination level and spatial frequency, and calculates information content (IC) representing the sum of the weighted spectral components at an arbitrary specified resolution. The algorithm produces an IC versus resolution curve providing a useful insight into the IC of an image for comparing between compression techniques. The HVS model, incorporated into this IQM, was experimentally optimized to provide the best correlation with subjective evaluations. However, this method is mainly designed for DCT coded images.

Nill and Bouzas [17] proposed an IQM derived from the image power spectrum. The measure assumes that the original image power spectrum is independent of content and therefore the image quality can be evaluated by its power spectrum. Their IQM incorporates an HVS model, and accounts for directional scale differences for obliquely acquired scenes. A modified Wiener filter is developed to account for imaging system noise. The IQM for an $M \times M$ pixels image is defined as:

$$\mathrm{IQM} = \frac{1}{M^2} \sum_{\theta=-180^\circ}^{180^\circ} \sum_{\rho=0.01}^{0.5} S(\theta_1) W(\rho) A^2(T\rho) P(\rho,\theta), \tag{4}$$

where $P(\rho,\theta)$ is the normalized 2-D power spectrum, ρ and θ are the radial spatial frequency and angle coordinates, respectively, $A^2(T\rho)$ is the square of the HVS modulation transfer function (MTF) with constant $T\rho$ subtended by the HVS, $S(\theta_1)$ is an IQM directional scale parameter with spatial frequency units, and W(ρ) is a modified Wiener noise filter. This IQM provides a single value that may distinguish between blur or noise existence only when separately added to the measured image, however its performances may be restricted by lack of knowledge that should be incorporated into the quality measure, when measuring an arbitrary image.

Wang and Simoncelli [23] showed a method for evaluating image blur using *phase coherence*, based on the observation that at sharp edges, phase information is highly ordered. Since blurring disrupts this local phase coherence behavior, the phases of non-sharp edges are no longer scale-invariant. The *phase coherence* across scales was evaluated in the wavelet transform domain. However, the results were obtained using also the original image for comparison. Also, it was not shown that this method can resolve fine differences in blur level.

3.2 NR quality measures in the spatial domain

Some image quality evaluation methods rely on perceptual features obtained in the spatial domain. High contrast sharp features such as edges, corners and texture may be more sensitive to specific degradations usually expressed as blur, and therefore can be used for image quality measurement for these cases.

Marziliano et al. [24] suggested an NR IQM specified for blur degradation using analysis of edge blurring in the spatial domain. It first finds vertical edges in the image and maps their locations. Then it defines the horizontal start and end positions of each edge according to the local extrema locations, closest to the edge. An edge width is derived from the distance between these extrema and is defined as the local blur measure for this edge location. A global blur measure is finally obtained by averaging the local blur values over all the edge locations. However, this measure depends on the quality of step-edges in the image.

Another method for measuring the quality of blurred images has been proposed by Ong et al. [25]. Their method computes the gradients' direction (divided into eight quadrants) for each pixel in the image. The extent of the slope of each of the edge pixels, in the two directions of the gradients' direction, is regarded as the edge-spread to indicate the amount of blur exhibited by each edge pixel. Finally, the image quality score is computed from the averaged edge-spread value. The method results are relatively well correlated with human subjective ratings.

For many motion blur cases, the blur extent may be a measure of the image quality, and can be blindly estimated from the degraded image [26]. More generally, the point spread function (PSF) can be a perfect degradation estimate when an image is degraded by a linear space-invariant blur. Various methods were developed for a blind estimation of the PSF in such a case [27]. However, these methods are specified for the motion-blur case, and assume a previous partial knowledge about the unknown PSF (such as one-dimensionality).

Noise estimation methods based on local variances were introduced in several studies [28–33]. Winkler and Süsstrunk [28] proposed a model for detecting a noise threshold on different types of image contents. They investigated the visibility of different types of noise in images using psychophysical experiments. Their model computes the lowest local standard deviation in a small region of the image (with the lowest activity, where noise visibility is higher). The calculated standard deviation is referred there as minimal σ_{image} representing noise visibility. Meer et al. [29] proposed an algorithm for noise variance estimation based on recursive computation of the local variance in increasing region sizes. For each recursive result the four smallest variance values are combined into a one estimate so that the sequential estimated values determine the noise variance of the image. Corner et al. [30] developed a noise estimation technique using data masking. Their method calculates a histogram of the local standard deviations over blocks after Laplacian filtering and edge-suppression using a Gradient mask. They experimentally discovered that the histogram median value supplied the most accurate final noise estimation. Another noise estimation histogram-based was presented by Rank et al. [31]. Amer et al. [32] introduced a fast white-noise estimation method by averaging the local variance values in the most homogeneous image blocks with similar homogeneities according to specified similarity threshold.

Li [33] proposed an NR image quality assessment technique by joining three different NR measures for three different image distortion types (blur, noise and block artifacts). The image blur is characterized by an objective measure of a *scale* parameter that determines the sharpness of an arbitrary oriented step edge at a detected step edges image. As scale parameter value increases it represents lower edge sharpness and thus a higher level of blur in the image. Noise percentage is estimated by detecting noisy pixels (based on the Least-Square adaptive predictive model) that violate the local smoothness constraint in the spatial domain. Block and ringing artifacts, are indicated from the overall edge detection ratio on block borders, and from the spectrum energy measured at high frequencies (ringing artifacts). This measure has not handle the interference between image features and

noise levels when attempting to simultaneously estimate the proposed three objective measures.

Brandão and Queluz [34] proposed a NR quality assessment metric for estimating quantization noise resulted due to lossy encoding such as JPEG or MPEG. Their proposed method is based on natural scene statistics of the DCT coefficients whose distribution may be modeled by a Laplace probability density function. The metric estimates original DCT coefficient distribution parameters from their quantized values and explores the correlation between coefficients distribution at adjacent DCT frequencies. Then, the resulting coefficient distribution estimations are used for estimating the local error and computing a quality score of the images. Their method has shown high correlation with human quality perception.

Gabarda and Cristóbal [35] propose a methodology for an NR metric to assess both the fidelity and quality of digital natural images. Their method is based on the multi-resolution information analysis of images that conclude that entropy per pixel is strictly decreasing with respect to decreasing resolution. The metric measures the averaged anisotropy of an image by means of a pixel-wise directional entropy. A pixel-wise directional entropy is obtained by measuring the variance of the expected Rényi entropy and the normalized pseudo-Wigner distribution (PWD) of the image upon a set of predefined directions. The measure is capable of distinguishing the presence of noise in images. The resulted image quality provided by the method is an index identifying in-focus, noise-free images from other degraded, blurred, or noisy versions. This method will be compared to the proposed method in Sect. 5.2.

4 Proposed NR assessment of blur or noise distortion impacts

The proposed method for NR assessment of the distortion impact on image quality assumes that the original image has common statistical properties largely independent of the image content. A distorted image degraded by blur and noise is commonly modeled for simplicity as affected by a linear, space-invariant blurring process and an additive noise: [8,16,26,36]

$$G(u, v) = F(u, v)\, H(u, v) + N(u, v), \tag{5}$$

where $G(u, v)$, $F(u, v)$, $H(u, v)$ and $N(u, v)$ are the Fourier transforms of the degraded image, the original image, the blurring PSF, and the additive noise, respectively.

As stated earlier, noise and blur distortions have contradicting effects on the statistical properties of the image. Noise (assumed to be wide-band) affects all spatial frequency bands and mainly increases the higher-frequencies, while blur mainly attenuates them. The proposed method uses common properties of natural images in both spatial and frequency domains, intending to identify and predict the impact of these distortions which may exist at the image. Noise impact on the image is evaluated in both spatial and frequency domains while blur is estimated only in the frequency domain. The method performs spectrum manipulations in order to evaluate the effect of the distortion in the frequency domain. The proposed method is summarized in Fig. 2, presenting an overall block diagram of the no-reference assessment process of noise and blur impacts on image. The figure is divided into three parts: Part A summarizes the noise estimation in the spatial domain (described in Sect. 4.1); Parts B and C summarize the noise and blur impacts estimation method in the frequency domain (described in Sects. 4.2 and 4.3).

4.1 Noise estimation in the spatial domain

Assuming a white Gaussian noise with zero mean, its power may be represented by its variance [16]. The noise power may be estimated from regions where the standard deviation of the original image is extremely small (non-significant activity in the original image). Areas with high activity are detected by thresholding the image gradient magnitude (obtained using a derivative-like operator such as Sobel) [30]. In order to reduce the detection of misleading (non-signal) high activity regions caused by noise, the image is first smoothed (with a small Gaussian kernel) prior to a gradient and thresholding operations. All the image areas above the threshold are considered to be areas with significant signal activities. As shown in Fig. 2 (Part A), the noise power is then estimated by dividing the image into overlapping square regions and averaging the variances of the regions contained in the below gradient-threshold areas. For the selection of parameters (the size of the blocks at which the noise is calculated from, and the threshold level), we followed the results obtained in Ref. [30] which removes the non-homogenous areas in the image using Sobel edge detector with a selected threshold. We examined the parameters used there over 20 different images and a wide range of the parameters. We found that the most accurate noise estimation results were obtained with parameters similar to those found in Ref. [30]. These parameters are block size of 10 pixels and a threshold of 4 (with an image gray-level range of 0–255). It should be noted that the noise power estimated in the spatial domain is not a measure of the noise impact on the image because the impact depends also on the image properties. The distortion impact assessment described below considers both, the distortion and the image properties.

4.2 Distortion impact estimation in the frequency domain

Noise and blur impacts on image quality are evaluated in the frequency domain using the image power spectrum. Blurring

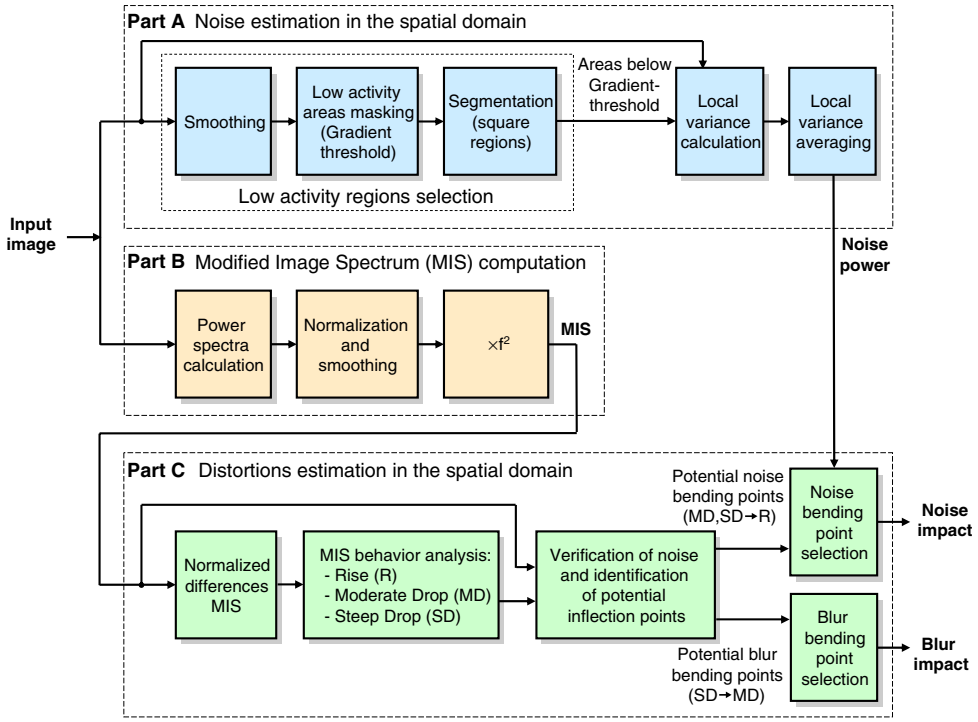

Fig. 2 Block diagram of the proposed no-reference assessment of noise and blur impacts on image

is a low-pass filtering phenomenon which obviously suppresses the higher spectral components. Noise, frequently assumed to be white, increases more significantly the image values at the higher frequencies since those are the lowest-energy components in the image spectrum. For the purpose of enhancing the visibility of these degradation effects when observing the image spectrum, we weight the degraded radial average image spectrum with a monotonically increasing function (with regard to the frequency coordinate). Since the dominant DC component (average of the image) does not contribute to the evaluation process, it is first removed. To illustrate the basic idea of the method, Fig. 3 presents a schematic diagram of the effect of a multiplication of an f^2 weighting function by degraded versions of a simplistic $1/f^2$ average image power spectrum model. The resulting multiplication becomes constant for the original image model (were no distortion exists in the image). It becomes an increasing function (positive slope) with regard to the frequency coordinate for the noisy image model, and a decreasing function (negative slope) for the blurred image model. When both noise and blur distortions exist in the image, the weighted spectrum model function may have both positive and negative slopes.

We define a *distortion bending point*, as a location at the weighted-spectrum which gives an evaluation of the distortion severity in the image, based on an analysis of inflection points in the curve (exact definitions of the blur and noise bending points are given in Sect. 4.3). The location of this bending point depends on the distortion severity. It depends

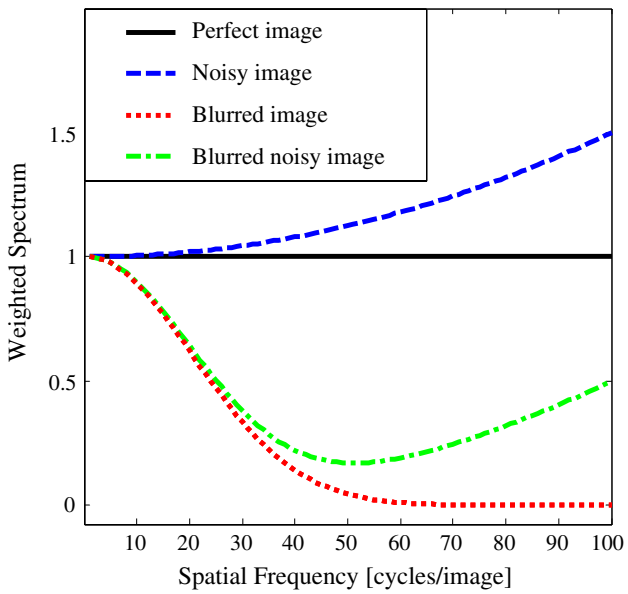

Fig. 3 Blur and noise effects on the multiplication of an f^2 weighting function by degraded versions of a simplistic $1/f^2$ image spectrum model. The weighted spectrum becomes constant for the original image model, an increasing function (*positive slope*) for the noisy image model, and a decreasing function (*negative slope*) for the blurred image model. When both noise and blur exist in the image, the weighted spectrum may have both positive and negative slopes

on the noise power in the case of a positive slope, and on the blurring severity in the case of a negative slope. As noise power or the blur severity is higher, the resulting bending

point is located at a lower frequency (more frequency components are significantly affected by the distortion). In order to prevent false local bending point detections, which may result from the random nature of a real image power spectrum, the power spectrum is first smoothed using an averaging convolution kernel. In order to enhance the visibility of the distortion effect, the smoothed power spectrum is then weighted by multiplying it with the squared spatial frequency f^2 to yield a *modified image spectrum* (MIS):

$$\mathrm{MIS}\,(f) = [P\,(f) * S]\,f^2, \tag{6}$$

where $P\,(f)$ is the normalized radial average (with respect to the angle) of the image power spectrum, S is the smoothing averaging kernel (up to 10% of the average spectrum length), and $*$ denotes a convolution operator. A schematic diagram of the MIS computation algorithm is shown in Fig. 2 (Part B).

The distortion type and impact are estimated according to the MIS. Although power spectra of different images are not identical, the general behavior of the spectra is quite similar. Generally, as the spatial frequency is higher, it contains less power, and it is significantly more affected by blur or noise. At these higher frequency components (beyond the distortion bending point), the spectrum shape is mostly affected by the distortion (manifested by the spectrum of the noise or the transfer function of the blur).

Figure 4 presents the MIS of the real image shown in Fig. 5a, and the MISs of different versions of it degraded by 3 levels of additive noise and 3 levels of defocus blur. Each MIS is normalized to a maximum level of one. The type of the degradations and their impact on the image can be observed from these graphs. The MIS graphs of the noisy versions are all above the MIS of the original, and as the noise level is higher, the resulting MIS bends at a lower frequency toward an increasing function at higher frequencies. The MIS graphs of the blurred versions are all below the MIS of the original, and as the blur size is larger, the resulting MIS bends at a lower frequency toward a flat function at higher frequencies. These behaviors of the MIS of a degraded image give a graphic indication of the degradation at the image, its type and its severity. The location of the global bending can give a quantitative estimation of the degradation severity.

4.3 Automatic calculation of blur and noise impacts

As presented in Fig. 2 (Part C), the bending point's location is selected from the MIS's potential inflection points. The algorithm identifies potential inflection points in the MIS by first calculating the normalized differences of the MIS's elements:

$$\mathrm{ND\_MIS}(i) = \frac{\mathrm{MIS}(i+1) - \mathrm{MIS}(i)}{[\mathrm{MIS}(i+1) + \mathrm{MIS}(i)]\,/2}. \tag{7}$$

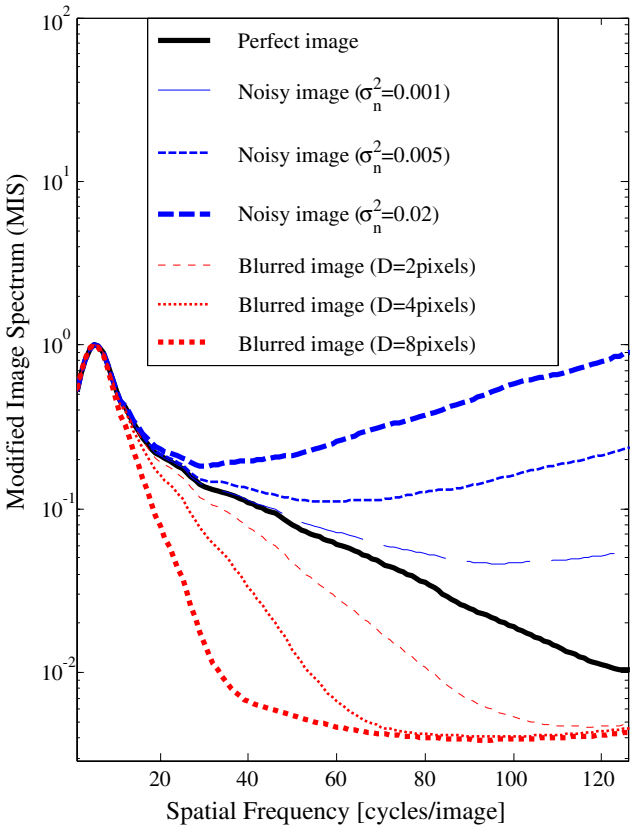

Fig. 4 Modified image spectrum (MIS) of a real image (shown in Fig. 5a) and the MISs of the image degraded by three levels of additive noise (*graphs above* the original) and three levels of defocus blur (*graphs below* the original). In all distortion cases, as the distortion level is higher, the resulting MIS bends at a lower frequency

Then it distinguishes between "rise", "steep drop" and "moderate drop" behaviors of the MIS as follows:

$$\text{Inflection behavior}\,(i) = \begin{cases} \text{"steep drop"}, & \mathrm{ND\_MIS}(i) < -\delta \\ \text{"moderate drop"}, & -\delta \le \mathrm{ND\_MIS}(i) \le 0 \\ \text{"rise"}, & 0 < \mathrm{ND\_MIS}(i) \end{cases}, \tag{8}$$

where δ defines a range in the ND_MIS (below zero) indicating the range of "moderate drop" behavior of the MIS, for the purpose of identifying potential blur bending points (changes from "steep drop" to "moderate drop"). A value of $\delta = 0.02$ was found empirically to produce reliable results.

An existence of significant noise in the image is decided if the noise power estimated in the spatial domain (Sect. 4.1) is above a certain threshold determined according to the minimum noise considered to be significant in the images. In our case this threshold was set up to be 0.001. Then, two cases are considered: significant noise (where both noise and blur bending points are considered), and non-significant noise (where only blur bending points is considered).

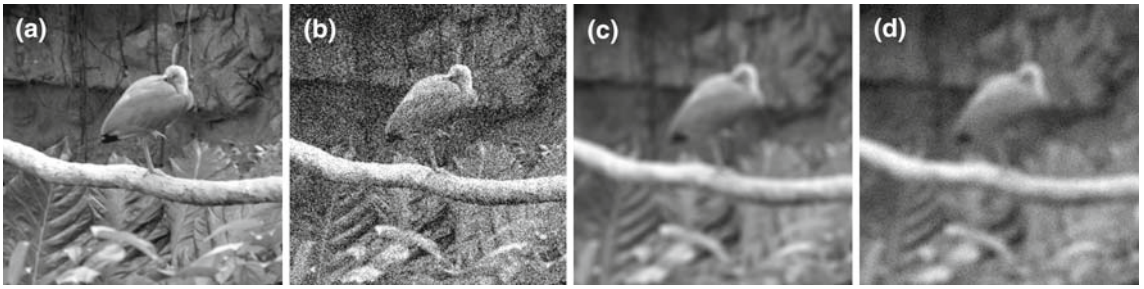

Fig. 5 Examples of degraded images generated from an original image **a**, and distorted by: **b** Gaussian white noise ($\sigma^2_{\text{input}} = 0.02$), **c** Defocus blur ($D = 8$ pixels), **d** Defocus blur ($D = 10$ pixels), and then Gaussian white noise ($\sigma^2_{\text{input}} = 0.001$)

- **Noise bending point extraction**: the *last change* from "drop" (steep or moderate) to "rise" in the MIS is a local minimum point considered to be the noise bending point. Since the white-noise power is about a constant while in a natural image the spectrum is strongly decreasing toward higher frequencies, the last section of the MIS curve (starting at the last significant inflection point) tends to be monotonically increasing. An example of an MIS of a noisy image with the selected noise bending point is shown in Fig. 6a, and its corresponding ND_MIS is given in Fig. 6c.
- **Blur bending point extraction**: the *first change* from "steep drop" to "moderate drop" in the MIS is an inflection point considered to be the blur bending point. This point usually reflects the behavior of the blurring MTF. Since blur reduces the higher frequencies of the image spectrum to zero or very close to that, the blur bending point location (that shows the beginning of a *suppressed spectrum region*) should be identified only at frequencies with very low-intensity of the spectrum. Therefore, a small threshold value is employed (about 2% above zero) to distinguish that *low-intensity spectrum region*. An example of an MIS of a blurred image with the selected blur bending point (identified within the *low-intensity spectrum region*) is shown in Fig. 6b, and its corresponding ND_MIS is given in Fig. 6d.

Note that the blur bending point is caused by two factors: The main factor is the shape of the MTF of the blur. The second is noise that exists at real images (which is not taken into account in the simplified $1/f^2$ image model). The shapes of various common blur MTFs are decreasing functions which reduce toward zero very fast (usually much faster than the image spectrum). Common blur MTF examples are: out of focus (Bessel function of order 1), a uniform velocity motion (Sinc function), harmonic vibrations (zero-order Bessel function), and atmospheric blur (approximated as Gaussian) [7]. Such blur functions together with the noise (usually considered white), multiplied by f^2, produce the blur MIS bending as defined above. The location of the bending is usually around the location of the first zero in the blur MTF or at a location where it reduces to a very low level. The noise, which produces an opposite effect to the blur, strengthens this phenomenon and may further create a turn of the MIS toward an increasing function at the highest frequencies.

4.3.1 Evaluation of the noise effect on image quality

Assuming a constant noise power and a decreasing image power (as stated earlier), when the noise power increases, the bending of the MIS (toward a positive angle) occurs at a lower frequency. This means that the number of image spectral components significantly affected by noise, defined here as the components beyond the noise bending point, increases with the increase in noise power. The ratio between the number of components mostly affected by noise and the total number of power components can estimate the noise impact on the image and thus it can be a measure of its noise-affected quality:

$$\text{Noise impact} = \frac{\text{Most noise affected components}}{\text{Total number of components}}, \tag{9}$$

The estimated noise impact value ranges between 0 and 1, where a higher value represents a higher noise impact.

4.3.2 Evaluation of the blur effect on image quality

As blurring extent grows, it is expected to significantly attenuate more power spectral components, resulting in an increased number of components beyond the blur bending point. The ratio between the number of components mostly affected by blur and the total number of power components may give a quantitative estimation of the blur impact on image and thus on its relative quality:

$$\text{Blur impact} = \frac{\text{Most blur affected components}}{\text{Total number of components}}. \tag{10}$$

The estimated blur impact value ranges between 0 and 1, where a higher value represents a higher blur impact.

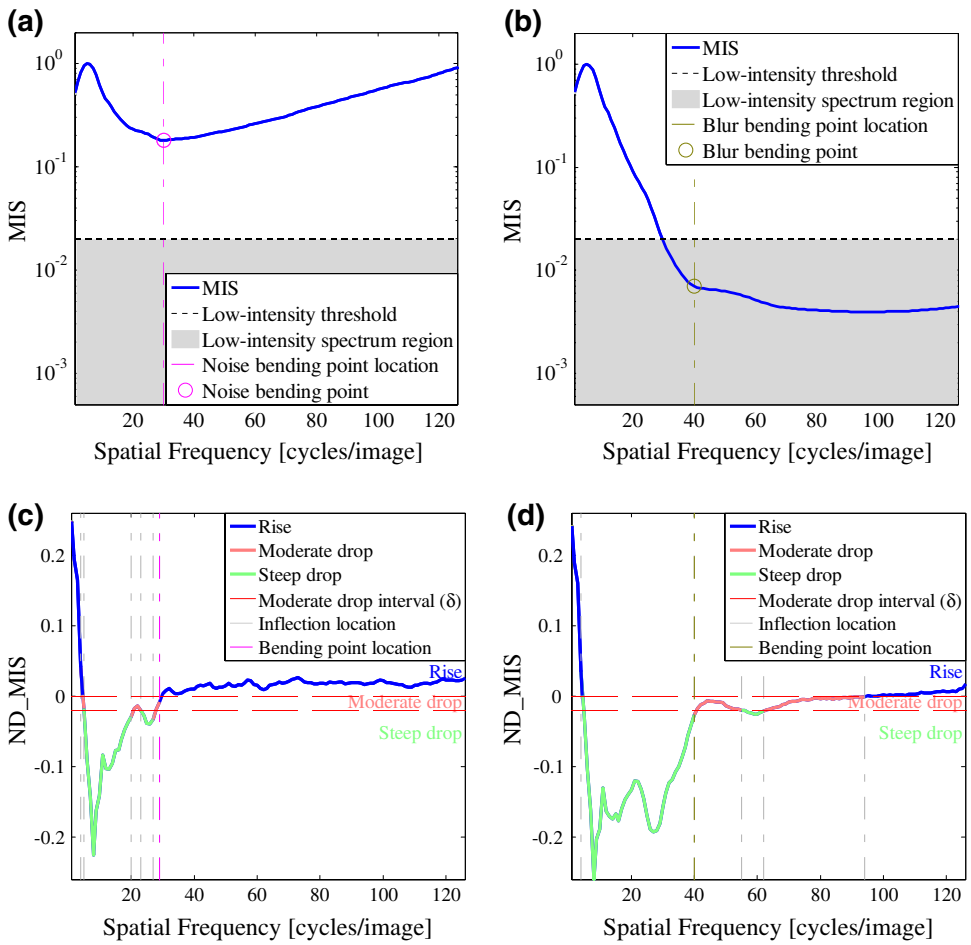

Fig. 6 Modified spectra and their identified bending points for an image degraded by additive Gaussian white noise (Fig. 5b), and Defocus blur (Fig. 5c). **a** The MIS and the selected bending point of the noisy image, obtained from the last change from "moderate drop" or "steep drop" to a "rise" of the MIS as shown in its corresponding ND_MIS (**c**). **b** The MIS and the selected bending point of the blurred image, obtained from the first change from "steep drop" to "moderate drop" of the MIS as shown in its corresponding ND_MIS (**d**)

5 Results

5.1 Proposed method performances

The method was examined with a set of 75 different monochrome 256 × 256 pixel natural images [11]. The test (original) images were used to generate images distorted by noise and blur, as shown in Fig. 5 for one of the images. The results of distortion impacts on image quality were derived using only the degraded images.

Results of noise power estimation in the spatial domain (as presented in Sect. 4.1), are shown here for five levels of additive Gaussian noise. Figure 7 presents the averages (over the whole image set) of the estimated noise variances for the different noise levels versus the true noise variances. It can be seen that for the lower noise levels, the estimated noise power is somewhat higher than the actual power. This behavior can be explained by the fact that the original images are not noise-free and their initial noise affects the results. For the highest noise levels (where the noise of the original

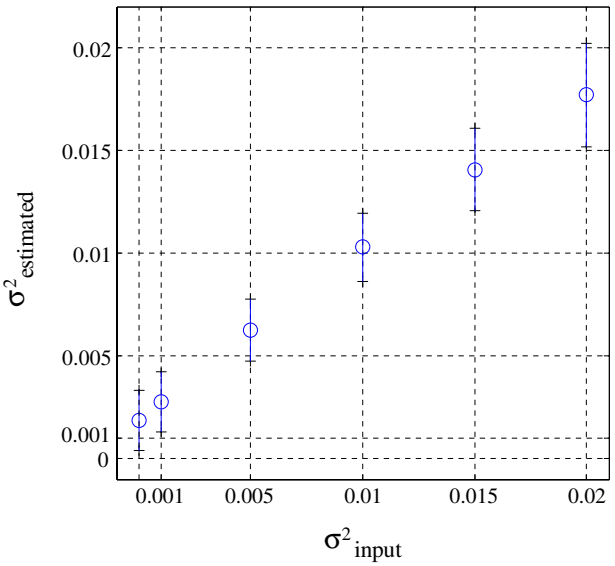

Fig. 7 Noise variance estimated values results and the related error obtained by 10 × 10 pixels block size and Sobel edge detector with threshold of 4, for the whole test images set

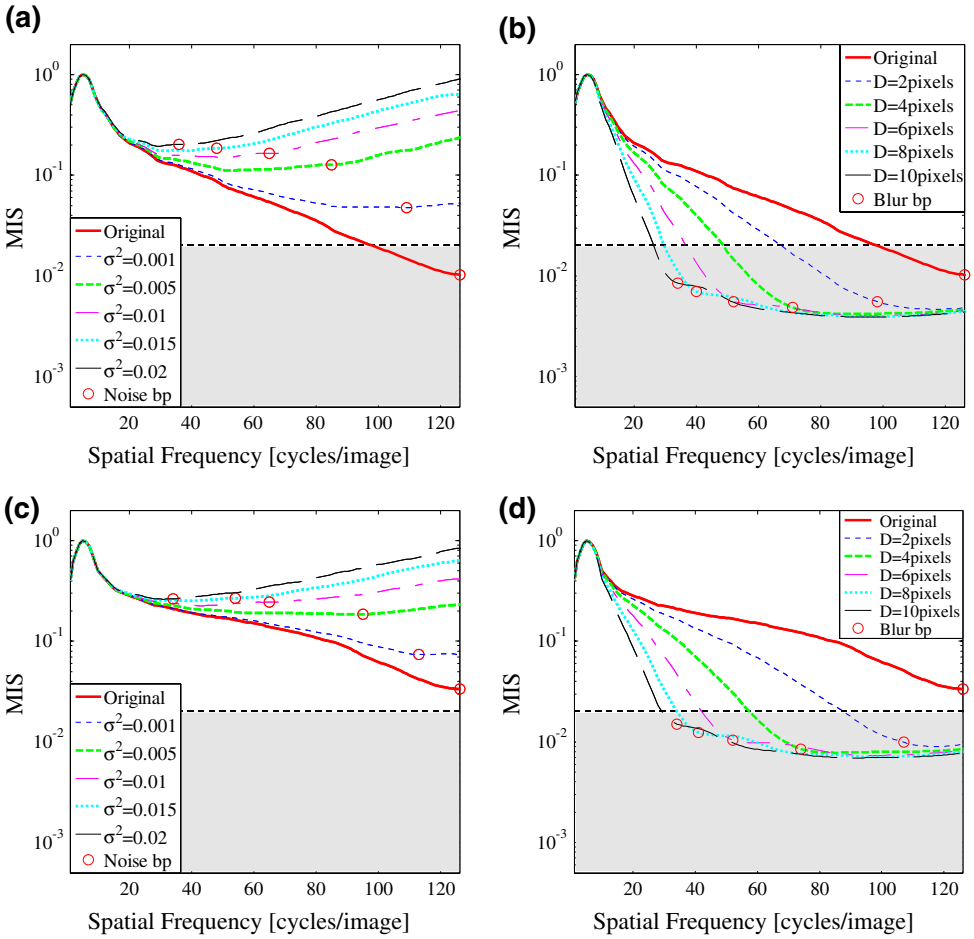

Fig. 8 Examples for the dependency of the bending point (bp) location on the distortion (blur or noise) level for two images. **a** the MISs and the selected noise bending points of the first image degraded by five different Gaussian white noise levels compared to the original spectra. **b** the same as **a** but for five sizes of defocus blur diameter D. **c** and **d** are the same as **a** and **b** but for the second image

image is not significant) the estimated noise power tends to be somewhat lower than the actual power. Better estimation results are obtained as the block size increases, due to the increased variability of the individual pixels caused by the noise [16]. Unfortunately, larger block sizes may meet difficulty in finding low activity regions since various images do not contain many large homogenous areas.

The performance of the proposed distortion impact assessment method, using the MIS presented in Sect. 4, was examined with different levels of three blur types (defocus, Gaussian and averaging) and a white zero-mean Gaussian noise. The bending point's location dependency on the distortion (blur or noise) level is demonstrated in Fig. 8 for two images (the first upper-left two images in Fig. 1). As shown in the graphs, the bending point is located at a lower frequency in the *MIS* as noise level increases, or as blur size enlarges. It can be seen from these examples that the locations of the bending points correspond to the noise power (in the noisy images) and to the blur extent (in the blurred images) even though the spectra of the original images (shown in each case) are different from each other. Figure 9 demonstrates that the locations of the bending points are consistent for different images (the 16 images presented in Fig. 1), for various levels of noise and various types and levels of blur.

When the evaluated image has strong periodic patterns, its MIS may be affected by the periodic components and therefore may result in a shifted noise bending point location. Usually the error in assessing the noise impact may be encountered by the spatial noise power estimation as explained in Sect. 4.1.

5.2 Both blur and noise in the image

The method performances might be limited when both blur and noise exist in the image. When the additive noise is relatively high, it will dominate the resulting MIS and the method will identify only the additive noise. This means that the method is limited (in the blur assessment case) to relatively low noise levels. Examples for cases of high and low noise levels at a blurred image are shown in Fig. 10. It can be seen that for the low-noise case (Fig. 10a, c), both bending points are identified, while for the high-noise case (Fig. 10b, d), the whole MIS graph is above the *low intensity spectrum region*, thus only the noise bending point is identified. A possible

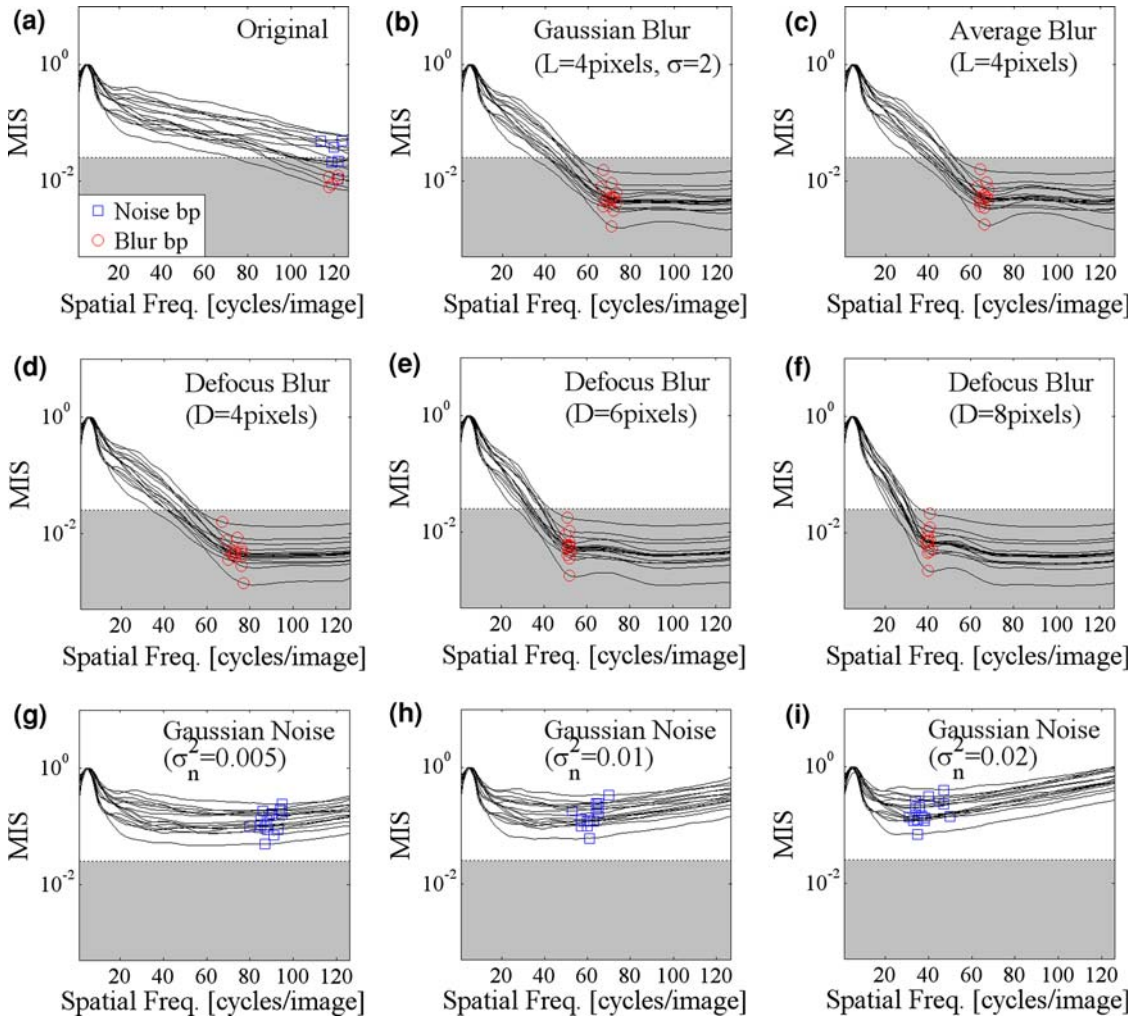

Fig. 9 MISs and their identified bending points for the 16 images presented in Fig. 1, degraded by the same distortion level: **a** Original images, **b** Gaussian blur ($\sigma = 2$ and 4 pixels kernel size), **c** An averaging blur of 4×4 pixels, **d** Defocus blur ($D = 4$ pixels), **e** Defocus blur ($D = 6$ pixels), **f** Defocus blur ($D = 8$ pixels), **g** Gaussian white noise ($\sigma^2_{\text{input}} = 0.005$), **c** Gaussian white noise ($\sigma^2_{\text{input}} = 0.01$), **d** Gaussian white noise ($\sigma^2_{\text{input}} = 0.02$)

solution for the high noise case may be to first de-noise the distorted image and then assess the blur impact. In such a case, since de-noising itself usually causes blur in the image, the blurring effect caused by the noise filtering should be taken into account.

5.3 Comparison results

The proposed method was compared to the recently developed method of Gabarda and Cristóbal [35], which performs Blind Image Quality Assessment through Anisotropy (BIQAA). The method concepts are briefly presented at the end of Sect. 3. It is a practical method and similarly to the proposed method, it considers both noise and blur distortion types, and employs the same methodology to assess the blur and the noise (unlike combining different methods to deal with noise and blur [33]). To obtain a similar range of an image quality score for both methods, the image quality score of the proposed method can be derived from the distortion impact presented in Sect. 4.2:

$$\text{Image quality score} = 1 - \text{Distortion impact}, \tag{11}$$

where the Distortion Impact value is obtained by Eqs. (9) and (10) for noise and for blur, respectively. This image quality score ranges from 1 (best quality) to 0 (worst quality). Figure 11 presents comparison results for three images (the first upper-left three images in Fig. 1). Table 1 shows the numerical comparison results. The methods were examined with different levels of defocus blur and Gaussian noise. As shown in the graphs, for both methods, the estimated image quality scores, for either noise (Fig. 11a) or blur (Fig. 11b), decrease as the distortion levels increase. It can be seen from

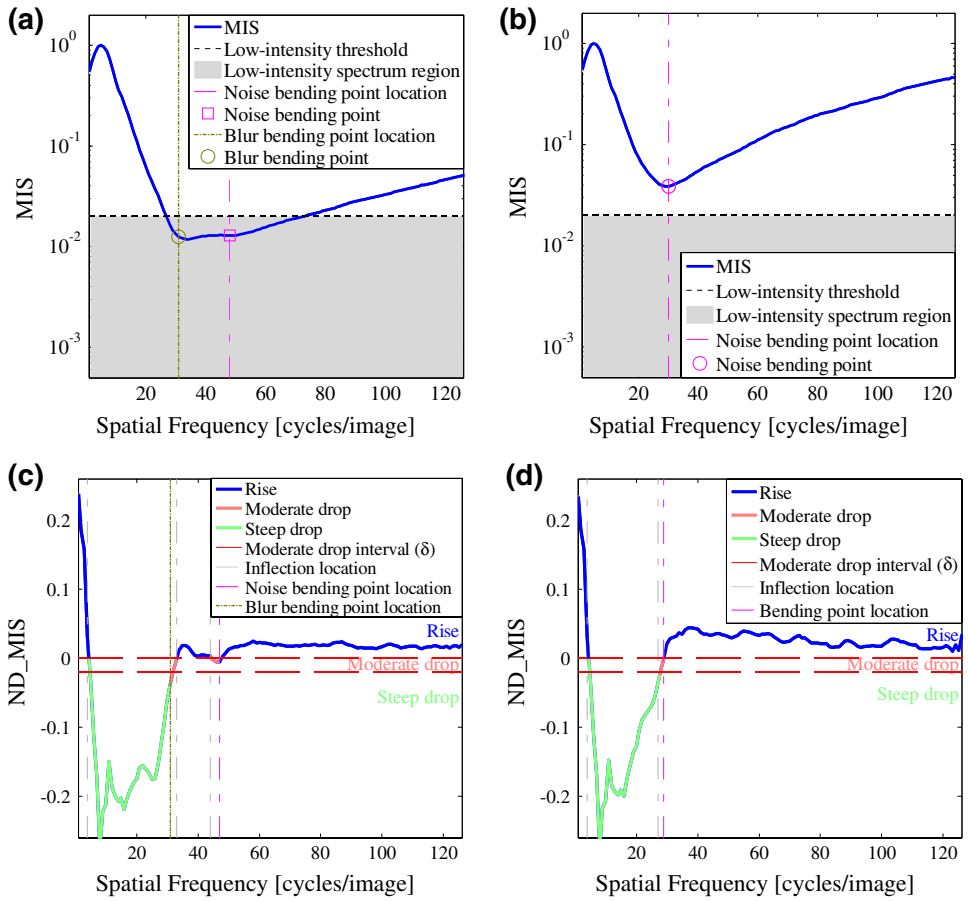

Fig. 10 MISs of two images degraded by both defocus blur ($D = 10$ pixels), and two levels of Gaussian white noise (low-noise and high-noise). **a** The MIS of the image (Fig. 5a) and the selected noise and blur bending points for the low-noise level ($\sigma^2_{\text{input}} = 0.001$), **c** The corresponding ND_MIS. **b** and **d** are the same as **a** and **c** but for the high-noise level ($\sigma^2_{\text{input}} = 0.01$)

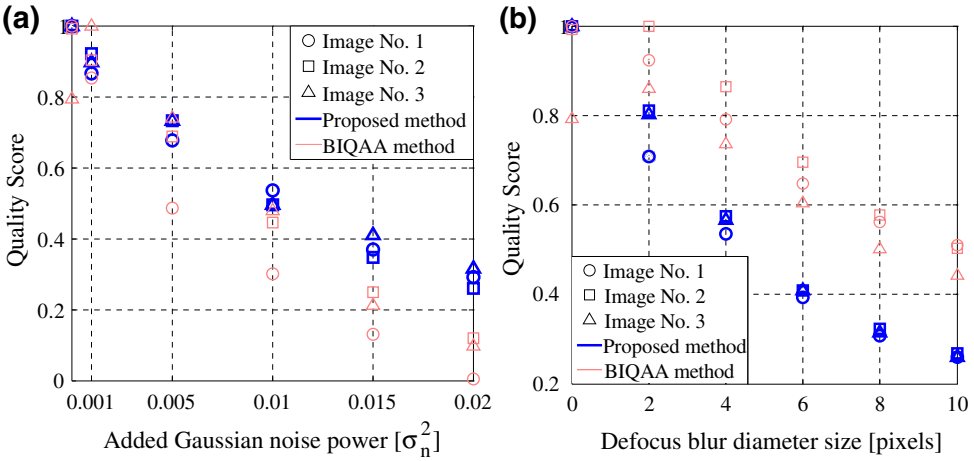

Fig. 11 Comparison of image quality results obtained by the proposed method and by the blind image quality assessment trough anisotropy (BIQAA) method presented in [35]. The image quality score are for three images degraded by different distortion levels: As degradation level increases the estimated quality score decreases. Five different Gaussian white noise levels are examined for each image in **a**, and five different defocus blur levels are examined for each image in **b**

these examples that the proposed method provided full consistency of the image quality scores with regard to the distortion levels, while few inconsistencies were obtained by the BIQAA method (as can be seen for image no. 3 with added noise power of 0.001 and for image no. 2 with defocus blur diameter of 2 pixels).

6 Conclusions

This paper presents a method for NR assessment of distortion impact on image quality based on common statistical properties of natural images. The method identifies the existence of noise and blur and estimates their impact on image

Table 1 Numeric image quality results obtained by the proposed method and the blind image quality assessment trough anisotropy (BIQAA) method presented in [35], for five levels of added Gaussian noise (a), and five levels of defocus blur diameters (b)

	Image no. 1		Image no. 2		Image no. 3	
	Proposed method	BIQAA	Proposed method	BIQAA	Proposed method	BIQAA
(a) Gaussian noise variance (σ^2_{input})						
0	1	1	1	0.99176	1	0.79324
0.001	0.86614	0.85342	0.92126	0.90307	0.89764	1
0.005	0.67717	0.48675	0.73228	0.68713	0.73228	0.74038
0.010	0.53543	0.30114	0.49606	0.44445	0.49606	0.47923
0.015	0.37008	0.13124	0.34646	0.24869	0.40945	0.21245
0.020	0.29134	0.00393	0.25984	0.11951	0.31496	0.09707
(b) Defocusing blur diameter (pixels)						
0	1	1	1	0.99176	1	0.79324
2	0.70866	0.92335	0.81102	1	0.80315	0.85991
4	0.53543	0.79139	0.57480	0.86366	0.56693	0.73618
6	0.39370	0.64768	0.40945	0.69619	0.40945	0.60382
8	0.30709	0.56237	0.32283	0.57770	0.31496	0.50149
10	0.25984	0.50932	0.26772	0.50346	0.25984	0.44303

quality. This is done by manipulating the image power spectrum in order to strongly enhance the distortion effect on the spectrum characteristics. Good and consistent results have been achieved for a variety of blurring types and sizes, and noise levels, when employed with different images. The method performances may be reduced in cases where the image contains strong periodic patterns and when a blurred image includes also high noise power.

References

1. Engeldrum, P.G.: Image quality modeling: where are we? In: IS&T's 1999 PICS Conference. Savannah, Georgia, pp. 251–255 (1999)
2. Wang, Z., Bovik, A.C., Lu, L.: Why is image quality assessment so difficult? In: Proceedings of Acoustics, Speech, and Signal Processing (ICASSP'02), 2002 IEEE International Conference, Orlando, vol. 4, pp. 3313–3316 (2002)
3. Wang, Z., Sheikh, H.R., Bovik, A.C.: Objective video quality assessment. In: Furht, B., Marqure, O. (eds.) The Handbook of Video Databases: Design and Applications, pp. 1041–1078. CRC Press, Boca Raton (2003)
4. Eskicioglu, A.M.: Quality measurement for monochrome compressed images in the past 25 years. In: Proceedings of Acoustics, Speech, and Signal Processing (ICASSP'00), 2000 IEEE International Conference, Istanbul, Turkey, vol. 4, pp. 1907–1910 (2000)
5. Avcibas, I., Sankur, B., Sayood, K.: Statistical evaluation of image quality measures. J. Electron. Imaging **11**(2), 206–223 (2002)
6. Eskicioglu, A.M., Fisher, P.S.: Image quality measures and their performance. IEEE Trans. Commun. **43**(12), 2959–2965 (1995)
7. Kopeika, N.S.: A System Engineering Approach to Imaging. SPIE Optical Engineering Press, Bellingham (1998)
8. Lagendijk, R.L., Biemond, J.: Basic Methods for Image Restoration and Identification. Academic Press, New York (2000)
9. Millane, R.P., Alzaidi, S., Hsiao, W.H.: Scaling and power spectra of natural images. In: Proceedings of Image and Vision Computing, New Zealand, pp. 148–153 (2003)
10. van der Schaaf, A.: Natural Image Statistics and Visual Processing. Ph.D. thesis, Rijksuniversiteit Groningen (1998)
11. Yitzhak Yitzhaky's Home Page at Ben-Gurion University, Israel. http://www.ee.bgu.ac.il/~itzik/nr_quality/ (2009). Accessed 12 May 2009
12. Huang, J., Mumford, D.: Statistics of natural images and models. In: Proceedings of Computer, Vision, and Pattern Recognition (CVPR'99). IEEE Computer Society Conference, vol. 1, pp. 1541–1547 (1999)
13. Reinhard, E., Shirley, P., Troscianko, T.: Natural image statistics for computer graphics. University of Utah, School of Computing. Tech report. UUCS-01-002 (2001)
14. Parraga, C.A., Troscianko, T., Tolhurst, D.J.: The human visual system is optimised for processing the spatial information in natural visual images. Curr. Biol. **10**(1), 35–38 (2000)
15. Castleman, K.R.: Digital Image Processing. Prentice-Hall, Englewood Cliffs (1979)
16. Lim, S.J.: Two-Dimensional Signal and Image Processing. Prentice-Hall, Englewood Cliffs (1990)
17. Nill, N.B., Bouzas, B.H.: Objective image quality measure derived from digital image power spectra. Opt. Eng. **31**(4), 813–825 (1992)
18. Torralba, A., Oliva, A.: Statistics of natural image categories. Netw. Comput. Neural Syst. **14**(3), 391–412 (2003)
19. Balboa, R.M., Grzywacz, N.M.: Power spectra and distribution of contrasts of natural images from different habitats. Vis. Res. **43**, 2527–2537 (2003)
20. Bex, P.J., Makous, W.: Spatial frequency, phase and the contrast of natural images. J. Opt. Soc. Am. **4**(6), 1096–1106 (2002)
21. Jain, A.K.: Fundamentals of Digital Image Processing. Prentice-Hall, Englewood Cliffs (1989)
22. Saghri, J.A., Cheatham, P.S., Habibi, A.: Image quality measure based on a human visual system model. Opt. Eng. **28**(7), 813–818 (1989)
23. Wang, Z., Simoncelli, E.P.: Local phase coherence and the perception of blur. In: Thrun, S., Saul, L., Schölkopf, B. (eds.)

Adv. Neural Information Processing Systems (NIPS'03), vol. 16 (2004)
24. Marziliano P., Dufaux F., Winkler S., Ebrahimi, T.: A no-reference perceptual blur metric. In: Proceedings of Image Processing, 2002 International Conference on Image Processing, Lausanne, Switzerland, vol.3, pp. 57–60 (2002)
25. Ong, E., Lin, W., Lu, Z., Yang, X., Yao, S., Pan, F., Jiarrg, L., Moscheni, F.: A no-reference quality metric for measuring image blur. In: Proceedings of Signal Processing and Its Applications, 2003 IEEE Seventh International Symposium, vol. 1(1–4), pp. 469–472 (2003)
26. Yitzhaky, Y., Milberg, R., Yohayev, S., Kopeika, N.S.: Comparison of direct blind deconvolution methods for motion-blurred images. Appl. Opt. **38**(20), 4325–4332 (1999)
27. Loyev, V., Yitzhaky, Y.: Initialization of iterative parametric algorithms for blind de-convolution of motion-blurred images. Appl. Opt. **45**(11), 2444–2452 (2006)
28. Winkler, S. Süsstrunk, S.: Visibility of noise in natural images. In: Proceedings of SPIE/IS&T Human Vision and Electronic Imaging, San Jose, CA, vol. 5292, pp. 18–22 (2004)
29. Meer, P., Jolion, J.-M., Rosenfeld, A.: A fast parallel algorithm for blind estimation of noise variance. IEEE Trans. Pattern Anal. Mach. Intell. **12**(2), 216–223 (1990)
30. Corner, B.R., Narayanan, R.M., Reichenbach, S.E.: Noise estimation in remote sensing imagery using data masking. Int. J. Remote Sens. **24**(4), 689–702 (2003)
31. Rank, K., Lendl, M., Unbehauen, R.: Estimation of image noise variance. In: IEEE Proceedings of Vision, Image and Signal Processing, vol. 146(2), pp. 80–84 (1999)
32. Amer, A., Mitiche, A., Dubois, E.: Reliable and fast structure-oriented video noise estimation. In: Proceedings of Image Processing, 2002 International conference on Image Processing, vol. 1, pp. 840–843 (2002)
33. Li, X.: Blind image quality assessment. In: Proceedings of Image Processing (ICIP2002), 2002 IEEE International Conference, vol. 1, pp. 1-449–1-452 (2002)
34. Brandão, T., Queluz, M.P.: No-reference image quality assessment based on DCT domain statistics. Signal Process. **88**(4), 822–833 (2008)
35. Gabarda, S., Cristóbal, G.: Blind image quality assessment through anisotropy. J. Opt. Soc. Am. **24**(12), B42–B51 (2007)
36. Hunt, B.R.: Image restoration. In: Ekstrom, M.P. (ed.) Digital Image Processing Techniques, pp. 53–76. Academic Press, Orlando (1984)